Additional information

Supplementary Information

Methodology for determining the key variables adopted as inputs for machine learning. To determine RBC shear modulus accurately, it is necessary to establish a quantitative relationship between the mechanical load and the resulting cell deformation. However, this is difficult to achieve for cells moving in a microchannel flow, where the viscous force and pressure on the cell are coupled with its deformability. The interaction force between the deformed cell and the surrounding liquid is expressed by integrating the local membrane stresses $f(s,t)$ in the corresponding Navier–Stokes equation. The force equals the increase in stress in the fluid field across the cell membrane, thus ensuring continuity of the stress in the flow field:

$$f(s,t) = (\sigma_{in} - \sigma_{out}) \cdot n = \nabla_s \cdot \tau$$

where s denotes the local curvilinear coordinates on the cell membrane, and σ_{in} and σ_{out} represent the internal and external stress tensors of liquids acting on the cell membrane, including pressure and viscous forces, respectively. The stress from the deformed cell contributes to the Navier–Stokes equation of the fluid-cell interaction as follows:

$$\rho\left(\frac{\partial u}{\partial t} + u \cdot \nabla u\right) = \nabla \cdot \sigma + \int_{\Gamma} f(s,t)\delta dS$$

where u, ρ, p, and μ are the fluid velocity, density, pressure, and viscosity of the flow field, respectively. Γ represents the surface region of the cell membrane. The complex interactions between the mechanical load and the deformation of the cell present significant challenges to direct measurement of cell shear modulus using a microfluidic device.

On the other hand, extracting cell shear modulus E_s from the details of the flow field in the microchannel is a complex and ill-conditioned problem.

$$E_s = f(\rho,p,\mu, u, D,\lambda,L, V,A...),$$

where λ is the thickness of the cell-free layer. To simplify the expression, we categorize all variables into different dimensionless groups using the Buckingham π theorem (in the Methods and Table S5). λ is negligible under bright field optical microscopy. The capillary number $Ca = \mu_{out}u_c/E_s$ is more strongly correlated with u_c/u_0 (r=0.687 and p=8.6×10^{-18}) and less strongly correlated with L/D (r=0.337 and p=1.9×10^{-4}) (Fig. S8). Here, μ_{out} is the fluid viscosity, u_0 is the fluid velocity in a microtube without cells,

and u_c is the steady-state velocity of the cell. Multivariate linear analysis of Ca using both u_c/u_0 and L/D yields a higher correlation coefficient (r=0.794 and p=1.4×10^{-25}), supporting the extraction of Es using these parameters.

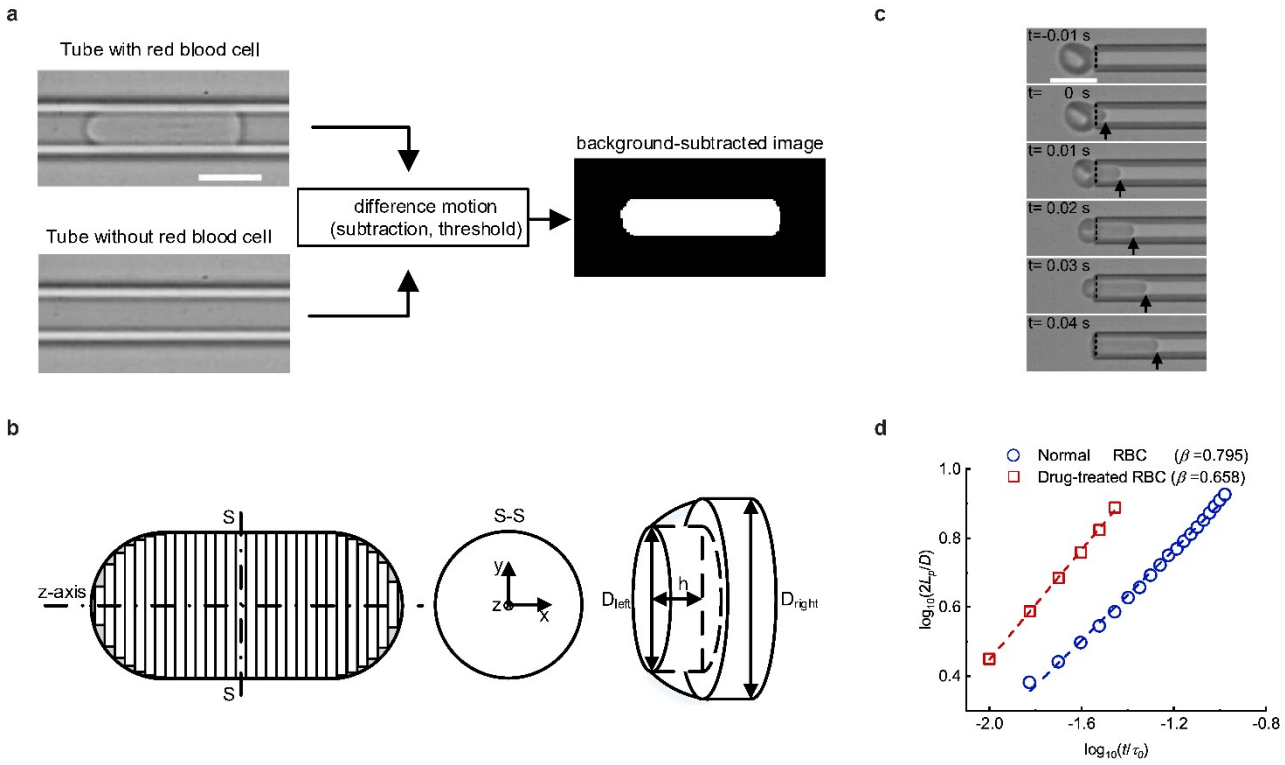

Fig. S1 Image processing for precise measurement of area, volume and viscosity. (a) Background subtraction to obtain the contour of a deformed RBC. Scale bar, 5 μm. (b) RBCs are discretized into frustum elements. The volumes and surface areas of the RBCs are calculated by summing the volumes and surface areas of the circular truncated cones, respectively. (c) Aspiration of an RBC at the entrance region with the high-throughput technique using a microtube with a diameter of 3.08 μm. Scale bar, 5 μm. (d) Estimation of the viscosity of the cell with power-law rheology. The squares and circles represent the data acquired in the experiments, and the slope of the line of fit is β. Here, the β value of normal RBC (red squares) is 0.80 (r^2=0.999), and the β value of drug-treated RBC (blue circles) is 0.66 (r^2=0.996).

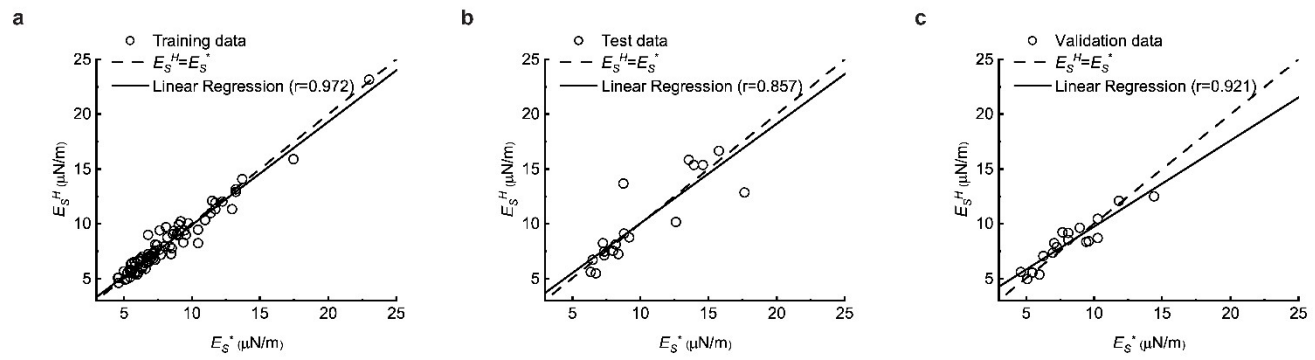

Fig. S2 Regression analyses of different datasets using the BP neural network. The dotted lines represent the ideal prediction where Es^H=Es^*. The solid lines represent the linear regression results.

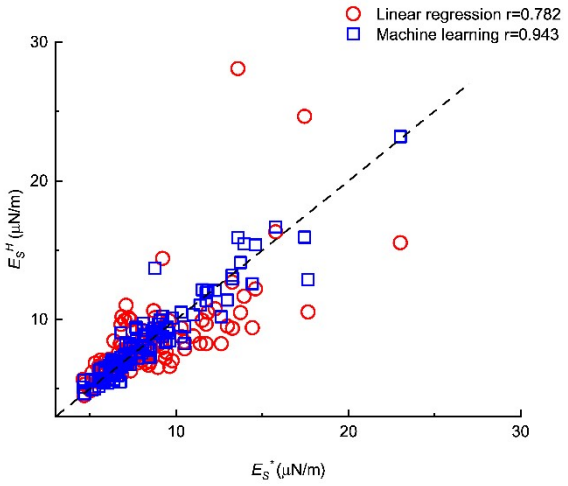

Fig. S3 Machine learning for predicting the shear modulus. This compares the correlation between the shear modulus measured by micropipette aspiration (Es*, ground truth) and the value (Es^H) predicted by two different methods: multiple linear regression (red circle, n=118) and the neural network (blue squares, n=118). The dotted line represents the ideal prediction Es^H =Es*.

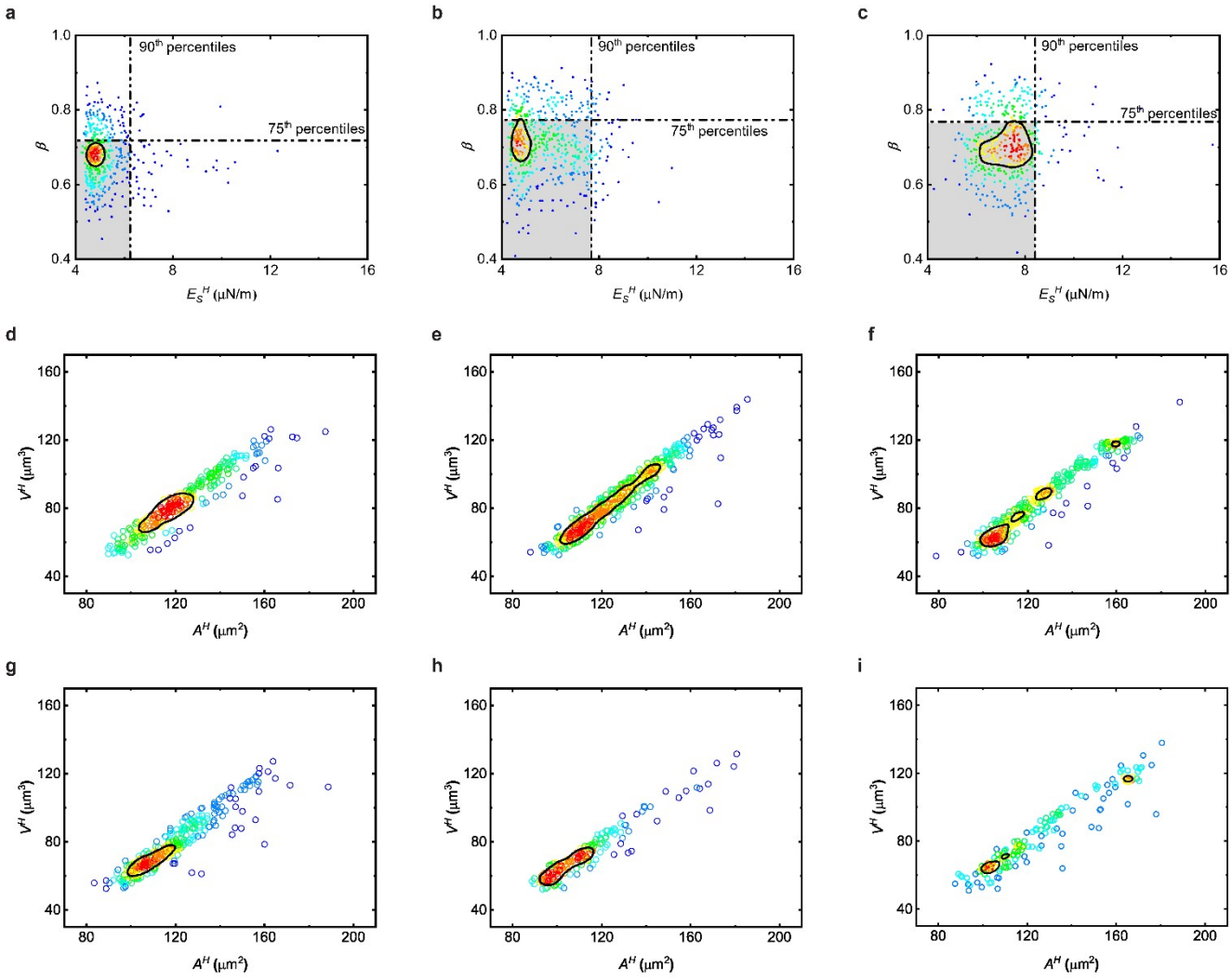

Fig. S4 Physical properties of RBCs in clinical blood samples with varying HbA1c levels. (a)-(c) Scatter plot of β versus Es^H for HbA1c levels of 7.1%(a), 8.6% (b) and 8.7% (c). The 75th percentile of β is represented by a double-dotted horizontal line, while the 90th percentile of Es^H is indicated by a double-dotted vertical line. The shadows indicate the areas of $Es^{H\alpha}\times\beta^{\gamma}$. The 70%-density contour lines are also displayed. (d)-(i) Scatter plot of surface area versus cell volume for HbA1c levels of 5.7%(d), 7.1% (e), 8.3% (f), 8.6% (g), 8.7% (h) and 9.6% (i). The 70% density contour lines are shown in black.

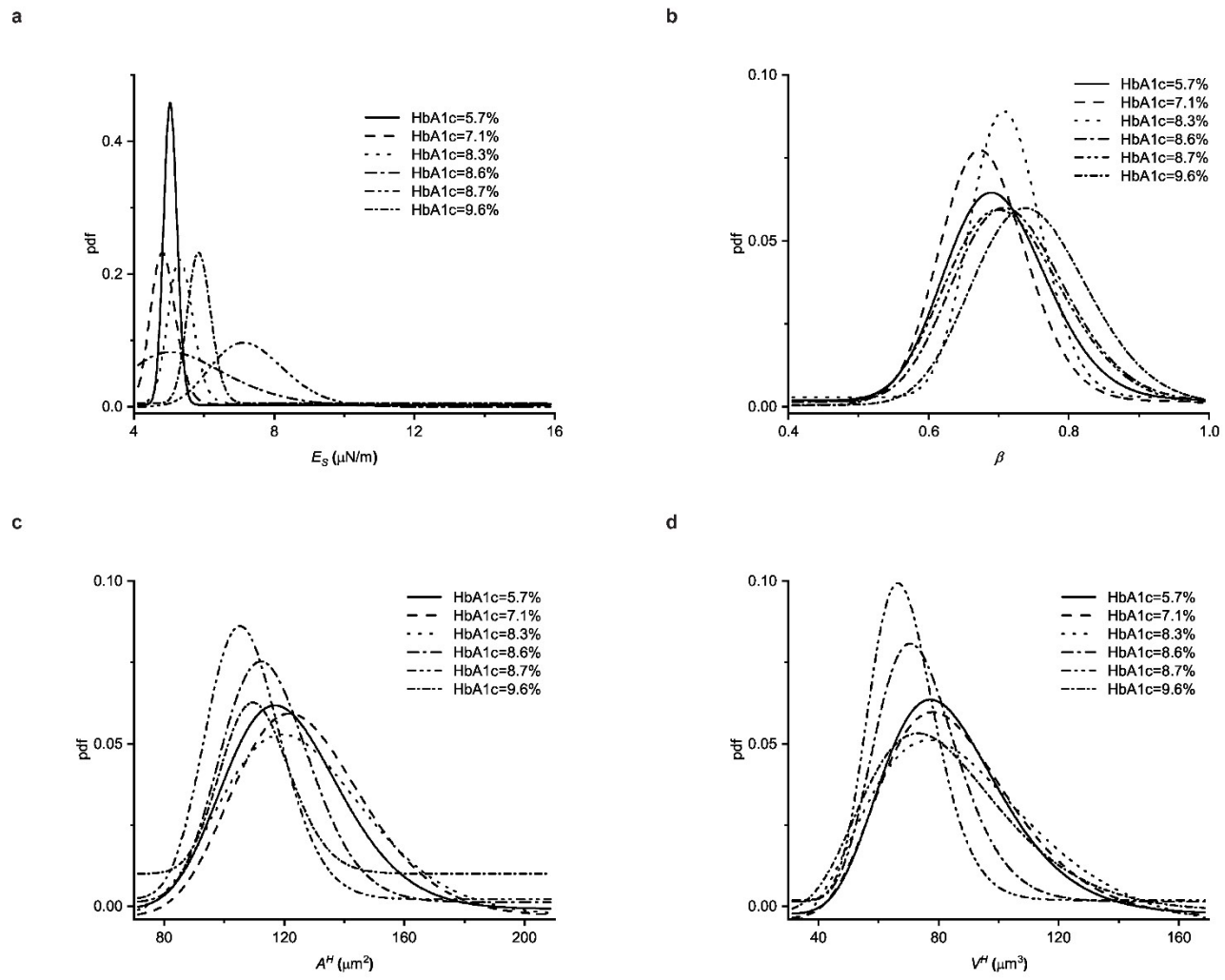

Fig. S5 Probability distribution functions for different physical properties. The lognormal fitting distributions of Es^H (a), β (b), A^H (c) and V^H (d) are shown with different lines representing various HbA1c levels.

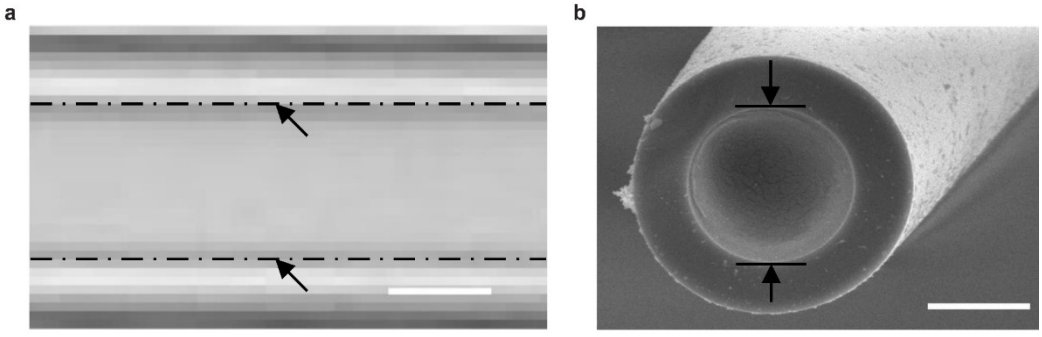

Fig. S6 Measuring the inner diameter of the microtube. (a) Bright-field optical microscope image with the position of the inner wall indicated by a dashed black line. Scale bar, 2 μm. (b) Scanning electron microscopy (SEM) image of the same microtube with the position of the inner wall indicated by a solid black line. Scale bar, 2 μm.

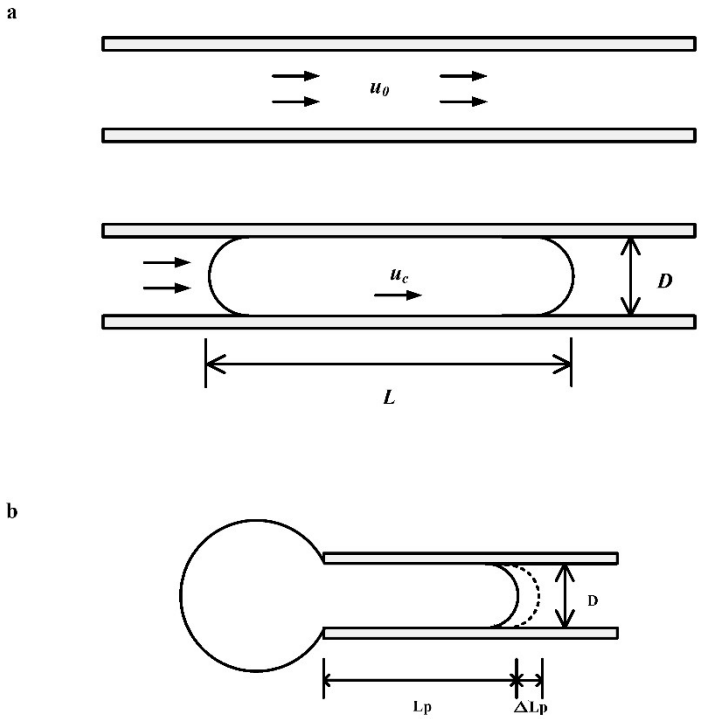

Fig. S7 (a) Schematic diagram outlining the four-parameter measurements of RBCs used in predicting shear modulus in a high-throughput method. (b) Schematic diagram of micropipette aspiration method for RBC membrane shear modulus.

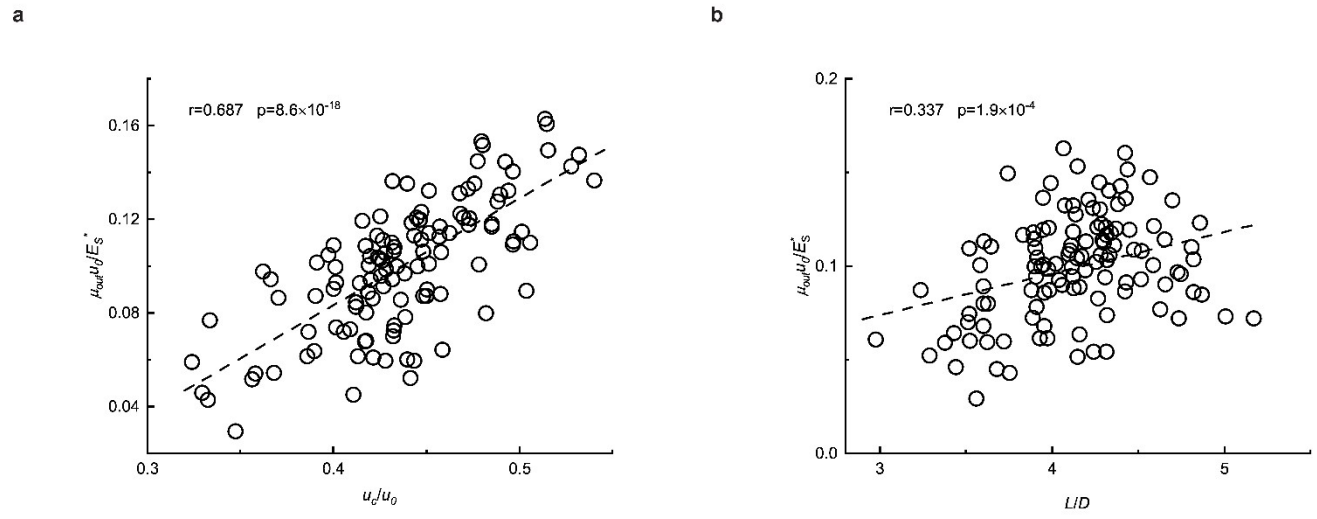

Fig. S8 Correlation analysis using dimensionless parameters. (a) Correlation analysis between the dimensionless shear modulus and the dimensionless cell velocity. The dotted line indicates the results of linear regression (r=0.689, p= 1.3×10^{-19}). (b) Correlation analysis between the dimensionless shear modulus and the dimensionless length of the RBCs under steady

deformation. The dotted line indicates the results of linear regression (r=0.337, p= 1.5×10^{-4}).

Video S1 The continuous motion of multiple RBCs in microtubes using the high-throughput method. The cells are aspirated and then move through the microtubes under constant negative pressure.

Table S1 Statistical analysis of drug effects on physical properties of RBCs.

Table S1 Statistical analysis of drug effects on physical properties of RBCs					
Diamide concentrations (mM)	Figure	Parameter	cohen'd	p value	Significance
0 vs. 0.1	Fig. 4a	E_s	2.27	1.30E-79	***
0 vs. 0.55	Fig. 4a	E_s	2.59	2.20E-164	***
0.1 vs. 0.55	Fig. 4a	E_s	0.38	1.53E-37	***
0 vs. 0.1	Fig. 4b	viscosity	1.04	5.07E-39	***
0 vs. 0.55	Fig. 4b	viscosity	0.81	1.76E-39	***
0.1 vs. 0.55	Fig. 4b	viscosity	0.24	0.0034	**
0 vs. 0.1	Fig. 4c	A	0.070	0.75371	ns
0 vs. 0.55	Fig. 4c	A	1.32	9.16E-30	***
0.1 vs. 0.55	Fig. 4c	A	1.42	1.45E-12	***
0 vs. 0.1	Fig. 4d	V	0.28	0.68361	ns
0 vs. 0.55	Fig. 4d	V	1.49	1.62E-32	***

0.1 vs. 0.55	Fig. 4d	V	1.86	2.37E-11	***

Table S2 Statistical analysis of physical phenotypes of RBCs at different HbA1c levels.

Table S2 Statistical analysis of physical phenotypes of RBCs at different HbA1c levels.					
HbA1c levels	Figure	Parameter	cohen'd	*p* value	Significance
5.7 vs. 7.1	Fig. 5a	E_s	0.043	1.92E-04	***
5.7 vs. 8.3	Fig. 5a	E_s	0.37	5.28E-57	***
5.7 vs. 8.6	Fig. 5a	E_s	0.42	8.14E-12	***
5.7 vs. 8.7	Fig. 5a	E_s	0.41	1.71E-159	***
5.7 vs. 9.6	Fig. 5a	E_s	0.80	8.94E-152	***
HbA1c levels	Figure	Parameter	cohen'd	*p* value	Significance
5.7 vs. 7.1	Fig. 5b	viscosity	0.16	0.00555	**
5.7 vs. 8.3	Fig. 5b	viscosity	0.29	3.12E-05	***
5.7 vs. 8.6	Fig. 5b	viscosity	0.25	1.33E-04	***
5.7 vs. 8.7	Fig. 5b	viscosity	0.24	0.00213	**
5.7 vs. 9.6	Fig. 5b	viscosity	0.71	1.11E-23	***
HbA1c levels	Figure	Parameter	cohen'd	*p* value	Significance
5.7 vs. 7.1	Fig. 5c	A	0.22	0.005	**

5.7 vs. 8.3	Fig. 5c	*A*	0.21	0.03297	*
5.7 vs. 8.6	Fig. 5c	*A*	0.22	0.00812	**
5.7 vs. 8.7	Fig. 5c	*A*	0.50	6.75E-09	***
5.7 vs. 9.6	Fig. 5c	*A*	0.21	0.33939	ns
HbA1c levels	Figure	Parameter	Z value	*p* value	Significance
5.7 vs. 7.1	Fig. 5d	*V*	0.097	0.31226	ns
5.7 vs. 8.3	Fig. 5d	*V*	0.14	0.24905	ns
5.7 vs. 8.6	Fig. 5d	*V*	0.29	4.21E-04	***
5.7 vs. 8.7	Fig. 5d	*V*	0.59	6.31E-10	***
5.7 vs. 9.6	Fig. 5d	*V*	0.076	0.97352	ns

Table S3 Correlation analyses with various percentile values of shear modulus and viscosity.

Table S3 Correlation analyses with various percentile values of shear modulus and viscosity.

Correlation / Value	r	P	Correlation / Value	r	P
Es^{H1th}	0.600	0.208	β^{1th}	0.522	0.288
Es^{H5th}	0.543	0.266	β^{5th}	0.706	0.117
Es^{H10th}	0.657	0.156	β^{10th}	0.812	0.0499*

Es^{H25th}	0.657	0.156	β^{25th}	0.754	0.0835
Es^{H50th}	0.886	0.0189*	β^{50th}	0.754	0.0835
Es^{H75th}	0.829	0.0416*	β^{75th}	0.928	0.00767**
Es^{H90th}	0.943	0.00481**	β^{90th}	0.841	0.0361*
Es^{H95th}	0.943	0.00481**	β^{95th}	0.812	0.0499*
Es^{H99th}	0.657	0.156	β^{99th}	0.928	0.00767**

Table S4 Information on the subjects and their health status.

Table S4 Information on the subjects and their health status.						
	Subject 1	Subject 2	Subject 3	Subject 4	Subject 5	Subject 6
Age	58	64	59	64	47	59
Gender	Male	Female	Female	Female	Male	Male
Glucose (reference, 3.9-6.1mmol/L)	5.41	8.98	9.37	4.91	8.74	11.28
HbA1c level (reference, 4.4-6.0%)	5.7%	7.1%	8.3%	8.6%	8.7%	9.6%
Relevant medication history	No	Liraglutide Dapagliflozin Acarbose	Metformin	Dapagliflozin, Saxagliptin, Prandial insulin	No	No

Table S5 List of physical parameters.

Table S5 List of physical parameters.		
Symbol	Description	Units
μ_{out}	Extracellular fluid viscosity	kg m^{-1} s^{-1}
ρ	Extracellular fluid density	kg m^{-3}
D	Inner diameter of the microtube	m
${E_S}^H$	Membrane shear modulus predicted by the high-throughput method	kg s^{-2}
${E_S}^*$	Membrane shear modulus measured with the micropipette aspiration method	kg s^{-2}
u_c	Velocity of a RBC moving at steady state in the microtube	m s^{-1}
u_0	Fluid velocity in a microtube without RBCs	m s^{-1}
L	Length of the deformed, steadily moving RBCs along the axis of the tube in the steady-state flow region	m
V	RBC volume	m^3
A	RBC surface area	m^2